

Satellite-based observations of surface turbulent stress during severe weather

Mark A. Bourassa

Center for Ocean-Atmospheric Prediction Studies and Department of Meteorology, Florida State University, USA

Abstract

Vector surface turbulent stresses are estimated from vector winds determined from space-borne scatterometers. Scatterometer vector winds differ subtly from *in situ* observations of vector winds. These differences are exaggerated for severe storm conditions, which is advantageous for determining surface stress. A physically based model for surface stress is developed to link surface turbulent stress to near-surface winds, and to explain the observed qualitative differences between *in situ* and scatterometer winds. The improvements of this model compared to previous formulations are in the near-surface boundary conditions on wind speed and a vertical offset (i.e., displacement height) of the log-wind profile, due to wave modification of the surface. The boundary condition on wind speed implies that there must be a vertical offset, and it can be used to derive the displacement height. This formulation represents a first estimate of the dependence of displacement height on wave characteristics. One advantage of this approach is that it removes sea state dependency from Charnock's constant. Strengths and weaknesses are discussed for this model and for its application in determining scatterometer-based vector surface turbulent stress.

1 Introduction

The environment of severe marine weather is harsh: *in situ* and satellite observations of surface turbulent stresses are extremely difficult to acquire under such conditions. Even for fair weather conditions, the spatial density of *in situ* observations is insufficient to examine the spatial and temporal evolution of mesoscale atmospheric systems. Satellite remote sensing provides an alternative that is capable of capturing the spatial structure of mesoscale atmospheric systems, although the temporal sampling is currently less than desired (Schlax *et al.* [1]). The lack of *in situ* stress observations is so severe that satellites are calibrated to measure winds rather than stresses, even though, since the planning stages the satellite era, it was believed that the satellite-borne instruments responded more to stress than to wind (O'Brien *et al.* [2]). Moreover, the frequency of occurrence of surface (10m) wind speeds greater than 16ms^{-1} is so rare that calibration of satellite instruments is suspect for wind speeds over about 20ms^{-1} . A further difficulty is that the calculation of surface stress, which is crucial for ocean forcing and momentum budgets on both sides of the air/sea interface, is complicated by the conversion of surface winds to surface turbulent stresses. For very large wind speeds, such as those found in hurricanes, there are several recent indications that the rate of increase in stress with increasing wind speed drops (Powell *et al.* [3]). Moreover, parameterizations of surface turbulent stress, which are calibrated for much lower wind speeds, tend to predict stresses that are too large when extrapolated to such extreme conditions. When such parameterizations are used in modeling strong hurricanes, the hurricanes weaken too fast due to excessive surface stress (Chen [4]). Satellite observations of winds will be discussed in section 2, and the conversion of wind speed to stress will be addressed in section 2.3.

Surface stress over water is primarily dependent on the vertical profile of wind speed, which is mainly dependent on wind speed differences between the sea surface and a known height. Secondary dependencies are the stratification of the atmosphere (atmospheric stability) and sea state (i.e., characteristics of the surface wave field). In severe weather, there can be great variations in sea state, both in the magnitude of the waves, and in the direction of wave propagation relative to the wind direction. Physical mechanisms have been proposed to account for the dependence of stress on sea state in many recent studies (Kusaba and Masuda [5], Geernaert [6], Toba *et al.* [7], Perrie and Toulany [8], Maat *et al.* [9], Smith *et al.* [10], Yelland *et al.* [11], Bourassa *et al.* [12], Bourassa [13]); however, an empirical formulation by Taylor and Yelland [14] based on a much wider range of wind speeds and non-directional sea states has been shown to provide a better match to mean observations that cover a wide range of conditions. Taylor and Yelland [14] acknowledge that while their model is a good match to the mean wind speed dependence, it leaves a great deal of

variability unexplained. A physically-based model that has a similar wind speed dependent mean and accounts for much more variability is discussed in Section 4.

Differences between satellite and *in situ* wind observations have been used to infer the relative importance of several wave characteristics by Quilfen *et al.* [15]. These results are expressed in terms of correlations among variables, which do not explain the physical mechanisms through which these wave characteristics modify surface fluxes. These wind observation differences also suggest that sea state parameterizations should be used to convert the *in situ* and/or satellite wind speeds to stresses. A physical mechanism that utilizes these insights was developed in the flux model of Bourassa [13] and found to be largely consistent with the results of Taylor and Yelland's [14] empirical relation. One advantage of this physically-based mechanism is that it also considers directional sea state (i.e., the wind direction relative to the directions of wave propagation). This additional consideration makes the flux model consistent with observations over a wider range of conditions. Concomitant non-directional impacts on surface turbulent stress, sensible heat, and latent heat fluxes are also discussed. These impacts can be substantial in severe weather.

2 Satellite observations of surface winds.

In the late 1990's, microwave scatterometry finally caught up to other radiometric instruments of the SeaSat satellite: altimeters (ocean height, wave height), radiometers (temperatures humidity, and rain), and scatterometers (wind speed and direction) were all designed to provide previously unattainable quantity and quality of data regarding variability of the ocean and adjoining atmospheric boundary-layer (Katsaros and Brown [16]). For example, the scatterometers on the European Remote Sensing Satellite Systems (ERS-1 and ERS-2) provided the first scatterometer data (starting in 1991) that could be used for climatological studies. However, operational constraints prevented continuous scatterometer observations while over water; which was where it was usually operating.

The Japanese satellite, ADEOS, was launched in August 1996 with the first dedicated microwave scatterometer since SeaSat: the NASA Scatterometer (NSCAT). This scatterometer determined wind speed and direction over 90% of the ice-free global water surface every two days, with 25-km in-swath grid spacing. It functioned until a catastrophic failure of the satellite platform occurred on June 29, 1997. Despite this loss, the unprecedented coverage and resolution of global wind data resulted in profound impacts on oceanographic and meteorological applications.

The unprecedented accuracy and coverage of NSCAT winds led to the rapid deployment of a new type of scatterometer (SeaWinds) to attempt to resume the

NSCAT-like observations. SeaWinds instruments were deployed on QuikSCAT (July 24, 1999 to present) and ADEOS-2 (April 10 to Oct. 22, 2003). SeaWinds scatterometers have approximately double the coverage of NSCAT, covering >90% of the world's oceans every day. The NSCAT and SeaWinds periods may be the only times to date when ocean modelers could *not* reasonably argue that errors in ocean model outputs were due mainly to shortcomings in wind observations. The short period when two SeaWinds scatterometers were operational provided approximately six-hourly coverage over most of the oceans.

2.1 Physics of Scatterometry

Scatterometers are unique among satellite remote sensors in their ability to accurately determine the wind speed and direction. Scatterometer microwaves are Bragg scattered by short water waves, which respond quickly to changes in winds. This backscatter (the fraction of transmitted energy that returns to the satellite) is dependent on wind speed and wind direction. The wind direction is found by determining the angle that is most likely to match that of the observed backscatters, using a digital filtering technique (Naderi *et al.* [17]) to rapidly sample small regions from multiple angles over a small period of time. There are substantial design differences among ERS scatterometers, NSCAT, and SeaWinds. For example, the ERS backscatter is spatially smoothed, thereby reducing the resolution to ~70 km (Freilich and Long [18]). The ERS satellites used three fixed antennas to scan the surface on one side of the satellite, whereas NSCAT had three fixed antennas on each side, allowing swaths on each side of the satellite track to be sampled by fore-, mid-, and aft- beams. NSCAT wind speeds and directions were calculated where there were radar observations from all three of these antennas, whereas ERS scatterometers were sometimes forced to use observations from only two antennas (Zecchetto *et al.* [19]). For fixed-antenna scatterometers (SeaSat, ERS-1/2 and NSCAT), the use of three or more antennas is essential for accurate determination of the wind direction (Naderi *et al.* [17]). The beam arrangement on SeaWinds instruments is a new design, with two conically rotating beams at fixed incidence angles. This design allows a single very wide observational swath. This scanning geometry has four substantially different angles over the portion of the swath similar to the NSCAT's coverage. However, near nadir and near the edges of the swath the angles are similar, resulting in decreased accuracy in these parts of the swath. Furthermore, only one of the two beams reaches the outer 100 km of the swath. These problems are somewhat compensated by a much greater observation density. NSCAT had three or four observations within a 25×25 km cell, whereas SeaWinds typically has between 8 and 15 observations within its 25×25 km cells.

The functions describing the wind direction are sinusoidal. Combining these functions to minimize the misfit usually results in multiple minima (ambiguous solutions often called ‘ambiguities’). Ideally, for fixed-antenna scatterometers, the best fit corresponds to the correct direction, the next-best fit is in approximately the opposite direction, and the next two minima are in directions roughly perpendicular to the wind direction. For SeaWinds scatterometers, the solution geometry varies across the swath. The solutions are similar to fixed-antenna scatterometer solutions in the part of the swath similar to NSCAT coverage, but differ greatly near nadir and near the swath edges. The process of choosing a direction from the multiple of possible solutions is called ambiguity selection. Noise and spatial/temporal variability can change the quality of fit and thereby cause incorrect directions (also known as aliases) to be chosen. NSCAT’s ambiguity removal skill was further improved by using two polarizations with one antenna, whereas SeaWinds ambiguity selection is improved by greater observation density. For NSCAT and QuikSCAT winds, a median filter (applied to ambiguity selection rather than wind direction) is also used to improve ambiguity selection.

An additional challenge is rain. Rain influences radar returns through three processes: backscatter from rain drops, attenuation of the signal passing through the rain (Weissman [20]), and modification of the sea surface shape by raindrop impacts (Bliven *et al.* [21], Sobieski and Bliven [22], Sobieski *et al.* [23]). The influence of these processes on the accuracy of winds is a function of scatterometer design. Rain has a greater influence at large incidence angles (the signal passes through more rain) and for Ku-band radar (NSCAT and SeaWinds) rather than C-band (ERS-1/2). Rain is not considered a serious problem for the ERS scatterometers. For NSCAT, rain contributed to substantial errors in the outer parts of the swaths, whereas for SeaWinds observations, rain can have a substantial influence throughout the swath. Modeling these problems is a concern in ongoing research (Weissmann *et al.* [20, 24], Yueh *et al.* [25], Draper and Long [26]).

2.2 Calibration and Equivalent Neutral Winds

Planning of post-SeaSat scatterometer missions assumed that scatterometers respond directly to surface turbulent stress rather than wind speed (O'Brien *et al.* [2]). The lack of sufficient calibration points for the direct determination of stress was foreseen, and it was decided to calibrate the instrument for the observation of surface (10m) wind. Co-located scatterometer and buoy winds were used to calibrate the scatterometer (Freilich *et al.* [27], Wentz and Smith [28]). More elaborate techniques were developed to ensure that a common reference scale was used to measure winds from three co-located types of observations (Stoffelen [29]). Winds determined with the NSCAT-1 geophysical

model function (Wentz and Smith [28]) have been validated against a wide range of *in-situ* and remotely sensed winds, and SeaWinds data have been validated with observations from research vessels (Bourassa *et al.* [30]).

Scatterometer wind speeds have been calibrated to 10m 'equivalent neutral wind speeds' (Cardone [31], Ross *et al.* [32], Cardone *et al.* [33], Verchell *et al.* [34]), which differ from surface wind speeds in a manner believed to be consistent with the physics to which the scatterometer responds. The differences can easily be explained with the equation for the modified log-wind profile:

$$\mathbf{U}(z) - \mathbf{U}_{\text{sfc}} = (\mathbf{u}_* / k) [\ln(z/z_o) - \varphi(z, z_o, L)], \quad (1)$$

where \mathbf{U} is the vector wind, \mathbf{U}_{sfc} is the velocity frame of reference (the surface current), \mathbf{u}_* is the friction velocity, k is von Karman's constant, z is the height above the local mean surface (10 m in this case), z_o is the roughness length, φ is a function of atmospheric stability, and L is the Monin-Obukhov scale length which is a measure of atmospheric stability. The response of scatterometers to the sea surface ($z \approx 0$), and the stability term (φ) is largely a function of z/L . Therefore, the accepted approach is to eliminate the stability term in the height adjustment. The equivalent neutral wind speed is parameterized in a manner similar to Eqn 1, and uses the same non-neutral values of \mathbf{u}_* and z_o ; however, the stability term (φ) is set to zero, implying

$$\mathbf{U}_{\text{EN}}(z) - \mathbf{U}_{\text{sfc}} = (\mathbf{u}_* / k) \ln(z/z_o). \quad (2)$$

Hence, the differences between $\mathbf{U}_{10\text{EN}}$ and \mathbf{U}_{10} are stability dependent,

$$\mathbf{U}_{10\text{EN}} - \mathbf{U}_{10} = \mathbf{u}_* \varphi(10, z_o, L) / k. \quad (3)$$

The kinematic surface turbulent stress is equal to the square of the friction velocity, and the friction velocity used in calibration of scatterometer winds should be the non-neutral value rather than the neutral value. However, values of $|\mathbf{U}_{10\text{EN}} - \mathbf{U}_{10}|$ are usually much less than 0.5 m s^{-1} , and relatively large values of $|\mathbf{U}_{10\text{EN}} - \mathbf{U}_{10}|$ tend to be associated with very stable stratification.

2.3 Determining Stress from Scatterometer Winds

The calculation of surface turbulent stress ($\boldsymbol{\tau}$) from wind speed also requires knowledge of the atmospheric stratification (Eqn 1).

$$\boldsymbol{\tau} = \rho \mathbf{u}_* | \mathbf{u}_* |, \quad (4)$$

The influence of atmospheric stratification on surface stress can be very large, particularly for stable stratification. The calculation of atmospheric stratification parameters requires knowledge of the air/sea temperature difference. Satellites can accurately determine sea surface skin temperature; however, on sub-synoptic time scales they are not yet effective in determining the temperature 10m above the surface.

One of the great advantages of equivalent neutral winds is that no knowledge of the atmospheric stability is required to determine surface stress. All that is needed is the density of the air and a neutral drag coefficient.

$$\boldsymbol{\tau} = \rho C_D \mathbf{U}_{10EN} |\mathbf{U}_{10EN}|, \quad (5)$$

The difficulties with this approach are the determination of the drag coefficient (described in section 3) and calibration of \mathbf{U}_{10EN} for severe weather. The calibration becomes an issue for wind speeds $>20 \text{ ms}^{-1}$ due to the lack of calibration data, and because of the interpretation of scatterometer winds. For wind speeds $>16 \text{ ms}^{-1}$, wave-related surface motion could become important in interpreting scatterometer winds (section 6).

3 *In Situ* Data

A preliminary analysis of observations from the Storm Wave Study experiment (SWS-2) was kindly provided by Peter K. Taylor (see also Dobson *et al.* [35], Taylor *et al.* [36]). These ship-based observations were gathered in the North Atlantic Ocean, with the goal of gathering a high quality data set for severe wind conditions. A key advantage of the data set is the existence of co-located buoy wave data. These observations have the additional advantage of covering a large range of wind conditions: 4 ms^{-1} to 24 ms^{-1} , with the quality control criteria described below. It is also the data set that Taylor and Yelland [14] used to demonstrate that models using the HEXOS parameterization (described by Smith *et al.* [10]) overestimated stresses for high wind speeds.

The following constraints were applied to the SWS-2 observations:

- 1) The sonic anemometer's estimate of the speed of sound is between 332 and 338 ms^{-1} ,
- 2) The standard deviation of the platform's heading is less than 14° ,
- 3) The dimensionless Monin–Obukhov scale length (z/L ; Eqns 4-6) is less than 0.18 .

These criteria serve as quality control on the stress and wave observations, as well as removing conditions that were too far from neutral to be considered. The first constraint ensures that the speed of sound, which is critical to the calculation of turbulent fluxes, is within the range expected from the observed air temperatures (Taylor [37]). The second constraint attempts to remove cases where excessive ship motion or flow distortion introduces too much variability

in the observations: approximately 1% of the observations are removed due to this constraint (Taylor [37]). The third constraint applies a measure of atmospheric stratification (z/L) to remove cases that are far from neutral stability, where the parameterizations that account for such departures are relatively uncertain.

4 Flux Model

The fluxes considered in this model are the downward momentum flux ($\boldsymbol{\tau}$), and the upward surface turbulent fluxes of sensible (H), moisture (E), and latent heat (Q). Stress can be modeled in terms of the friction velocity (\mathbf{u}_*):

$$\boldsymbol{\tau} = \rho \mathbf{u}_* |\mathbf{u}_*|, \quad (6)$$

where ρ is the density of the air. Sensible heat, moisture, and latent heat fluxes are

$$H = -\rho C_p \theta_* |\mathbf{u}_*|, \quad (7)$$

$$E = -\rho q_* |\mathbf{u}_*|, \quad (8)$$

$$Q = -\rho L_v q_* |\mathbf{u}_*| = L_v E, \quad (9)$$

where θ_* and q_* are scaling parameters analogous to u_* , C_p is the specific heat of air, and L_v is the latent heat of vaporization. The following considerations improve the accuracy of these modeled surface turbulent fluxes by improving the accuracy of modeled values of u_* .

The direct influence of surface waves on flux and airflow characteristics (\mathbf{u}_* and z_o) is determined by the relation between \mathbf{u}_* and roughness length (z_o). Given $z_o(\mathbf{u}_*)$ and the modified log wind relation $\mathbf{U}(z)$, where z is the height above the local mean surface, it is possible to iteratively solve for $\mathbf{u}_*(\mathbf{U})$ and $\boldsymbol{\tau}(\mathbf{U})$. The modified log-wind relation is

$$\mathbf{U}(z) - \mathbf{U}_s = \frac{\mathbf{u}_*}{k} \left[\ln \left(\frac{z-d}{z_o} + 1 \right) + \phi(z, z_o, L) \right], \quad (10)$$

where k is von Kârmân's constant, d is the displacement height (the height at which the log wind profile extrapolates to zero wind speed), and L is the Monin-Obukhov stability length. The influence of atmospheric stratification in the boundary-layer is modeled through the Monin-Obukhov stability length (Liu *et*

al. [38]). The profiles of potential temperature (θ) and specific humidity (q) have functional forms similar to the log-wind profile. The parameterization of momentum roughness length (Eqn 12) is adapted from Bourassa [13], and the roughness lengths for potential temperature ($z_{o\theta}$) and specific humidity (z_{oq}) are adapted from the surface renewal model of Clayson *et al.* [39], which implies that they are proportional to the momentum roughness length. The parameterization of L is identical to that used in the BVW (Bourassa-Vincent-Wood) flux model [12], the CFC (Clayson-Fairall-Curry) model [39] and also Bourassa [13].

4.1 Momentum Roughness Length

There have been many attempts to model the dependence of stress on sea state. Many of these studies have followed the suggestions of Charnock [40], who used dimensional analysis to parameterize momentum roughness length:

$$z_o = a u_*^2 / g, \quad (11)$$

where a is a dimensionless parameter (now called Charnock's constant) that is often considered to be a function of sea state conditions. The wave dependence in subsequent models of surface turbulent stress typically enters through Charnock's constant in the gravity wave contribution to the roughness length parameterization (see Kusaba and Masuda [5], Geernaert [6], Toba *et al.* [7], Perrie and Toulany [8], Maat *et al.* [9], Smith *et al.* [10], Bourassa *et al.* [12]). The momentum roughness length parameterization used here (Bourassa [13]) is a modification of that of BVW [12]. BVW stresses were found to greatly overestimate the high wind speed stresses observed in SWS-2 as discussed by Dobson *et al.* [35], Talyor *et al.* [36], and Taylor [41]. It was speculated (Bourassa *et al.* [12], Taylor [41]) that these biases were due to extrapolating the HEXOS parameterization for momentum roughness length (Smith *et al.* [10]) to conditions for which it was not valid. The roughness length parameterization used here, given in Eqn 12, can be written with no explicit dependence on sea state, where the gravity wave roughness length is a two-dimensional version ($i = 1, 2$) of Charnock's relation [40]

$$z_{o_i} = \left[\beta'_v \frac{0.11\nu}{|u_{*i}|} + \left[\left(\beta'_c \frac{b \sigma}{\rho_w |u_*| |u_* \bullet \hat{e}_i|} \right)^2 + \left(\beta'_g \frac{a |u_*| |u_* \bullet \hat{e}_i|}{g} \right)^2 \right]^{0.5} \right] \quad (12)$$

Here, the β terms are binary weights for the roughness lengths (from left to right) associated with contributions to surface roughness from three types of surface features: an aerodynamically smooth surface (Nikuradse [42], Kondo [43]), capillary waves (Bourassa *et al.* [12]), and gravity waves (Smith *et al.* [10]), where ν is the molecular viscosity of air, b is a dimensionless constant (determined from laboratory observations), σ is surface tension, ρ_w is water density, and g is gravitational acceleration. The influence of sea state enters solely through the modification of vertical shear in wind speed, given in Eqn 13, due to a non-zero lower boundary condition, the wave-induced surface motion

$$[U(z) - fU_{orb} - U_{current}] \cdot \hat{e}_i = \frac{u_* \cdot \hat{e}_i}{k} \left[\ln \left(\frac{z-d}{z_{o_i}} + 1 \right) + \varphi(z, z_o, L) \right]. \quad (13)$$

The roughness length is therefore anisotropic, with unit vectors parallel (\hat{e}_1) and perpendicular (\hat{e}_2) to the mean direction of wave motion. The orbital velocity (U_{orb}) term transforms the velocity frame of reference to that of a fraction f of the orbital velocity of the dominant waves. Laboratory studies (Okuda *et al.* 44]) have shown that most of the interactions between wind and wind-driven waves occur near the crest of the dominant waves. This process is modeled by modifying the lower boundary condition on velocity. The orbital speed of gravity waves is approximated by

$$U_{orb} = \pi H_s / T_p, \quad (14)$$

where H_s is the significant wave height, and T_p is the corresponding significant wave height period. For gravity waves, U_{orb} can easily be related to the significant slope used by Taylor and Yelland [14]. The fraction of the orbital velocity (f) that modifies the surface wind was set at 80%, following Bourassa [13]. The value of 0.8 applies to wind-driven waves: flow separation can be much less important for swell than for wind driven waves, suggesting that the value for f should be smaller for most swell conditions.

The use of significant wave height in Eqn 14 is an oversimplification: H_s can be a combination of wind waves and swell from multiple sources. Directional differences in the wave spectra will contribute to errors in the estimated orbital velocity and consequently, to errors in the stresses. However, wave spectra are rarely available from observational studies; whereas H_s is frequently recorded *in situ* observations, and is remotely sensed through satellite altimetry. In practice, there are few sources of spectral wave information other than from wave models (for example WAM model outputs as noted by Günther *et al.* [45], and Janssen

[46,47]) as implemented in operational weather centers. The lack of wave directional information in the SWS-2 data, and hence the lack of consideration in this study, presumably causes a substantial fraction of the unaccounted variability in the SWS-2 data.

Bourassa [13] pointed out that the roughness length could be given a more conventional form by moving the fU_{orb} term from the left hand side of Eqn 13 to the roughness length in Eqn 12. However, that is inappropriate here because the roughness lengths for potential temperature and moisture are dependent on the roughness length for momentum. Comparisons of modeled and observed sensible and latent heat fluxes (not shown) support the form of roughness length used in Eqn 13.

4.2 Displacement Height

The displacement height is not considered as another free parameter: it is derived as part of the lower boundary condition on the log-wind profile. Several derivations of the modified log-wind profile lead to Eqn 15 after integrating from the smallest length scale of eddies to the length scale associated with an arbitrary height z .

$$\frac{\partial \bar{u}}{\partial z} = \frac{\sqrt{\tau / \rho}}{k_v} \frac{1}{(z - z_o)} \quad (15)$$

The modified log-wind profile is then found by integrating Eqn 15 from the height where the surface relative wind speed extrapolates to zero, to the wind speed at a height z

$$\bar{u} \Big|_{z=d}^{z=z} = \frac{\sqrt{\tau / \rho}}{k_v} \log \left(\frac{z}{z_o} + 1 \right) \Big|_{z=d}^{z=z}. \quad (16)$$

Hence the bottom boundary condition, $\bar{u}(d)$ corresponds to the frame of

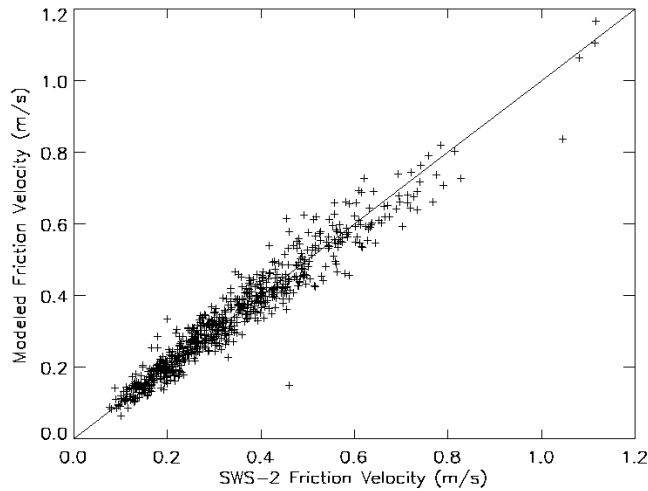


Figure 1: Comparison of modeled and observed SWS-2 friction velocity magnitudes, shown as a scatter plot

reference for the wind speed. This frame of reference was found to be approximately 80% of the magnitude of the orbital velocity of the dominant wind-waves (Bourassa [13]). The displacement height is then the height that corresponds to this speed: 80% of the significant wave height (fH_s) for wind-driven waves. This value of the displacement height follows directly from the derivation of the modified log-wind profile and knowledge of the frame of reference for wind speed. The orbital velocity term usually reduces the stress by decreasing the wind shear. In contrast, the displacement height acts to increase the wind shear.

5 Comparisons to observations

The model is evaluated with SWS-2 observations, because this data set is of the highest quality and should therefore provide an important calibration. In particular, all the required meteorological data, flux data, and wave data were recorded (although directional wave information is not available for this study). As the surface water is well mixed, the differences between bulk and skin temperature can safely be ignored. These are important considerations, because they remove substantial biases in both friction velocity and the sea surface temperature (SST).

Charnock's constant is highly dependent on the velocity frame of reference ($f\mathbf{U}_{\text{orb}} + \mathbf{U}_{\text{current}}$) and the displacement height (d): a small percentage change in $|\mathbf{u}_*|$ corresponds to a large percentage change in z_o . This approach reduces the root-mean-square (rms) differences between modeled and observed friction velocity from 0.078 to 0.041 ms^{-1} . Displacement height was not considered by Bourassa [13], and it was found that $f=0.8$ and $a=0.064$ resulted in a good fit to the SWS-2 data, particularly in the mean. However, this result was highly influenced by observations at extreme wind speeds ($U_{10} > 15 \text{ ms}^{-1}$), where the displacement height was relatively significant. A different value for Charnock's constant would be found if the extremely strong wind speeds or large wave heights were excluded. The change in modeled values of u_* due to this uncertainty in the value of Charnock's constant is small for SWS-2 data with $7 < U_{10} \leq 15 \text{ ms}^{-1}$. Although the application of any model to conditions for which it was not tested is always problematic, it is necessary in the absence of appropriate data. Models with more detailed physical considerations are more likely to result in an accurate extrapolation into untested conditions. Here, consideration of d results in $a=0.035$ (Fig. 1), with a very good match to the means shown in Fig. 2 except for the most extreme conditions where the sample size is relatively small. Furthermore, these values for f and a are found for any reasonably large sub-range of wind speeds or friction velocities from the SWS-2 data.

There is considerable spread about the means (Fig. 2), which is expected in part due to the lack of directional sea state information. The rms difference between modeled and observed values is 0.041 ms^{-1} , when the orbital velocity and displacement height are considered, and increases to 0.078 ms^{-1} when these considerations are ignored. The median value of the absolute value of the relative error is 11% when orbital velocity and displacement height are considered. Remarkably, the consideration of orbital velocity has also been demonstrated by Bourassa *et al.* [12] to account for observed variability in surface stress for conditions of low wind speeds and old swell, as noted by Donelan *et al.* [48].

The influences of $u(d)$ and d on the friction velocity are demonstrated with the SWS-2 data in Fig. 3. Although the wind speed modification tends to dominate for wind speeds throughout the range of conditions shown, the influence of this modification in the SWS-2 data is approximately a constant proportion of the magnitude of the friction velocity. The influence of displacement height is very small (Fig. 3) for friction velocities below approximately 0.55 ms^{-1} (wind speeds below approximately 12 ms^{-1}). However, it increases with increasing SWS-2 friction velocity (and increasing wave heights).

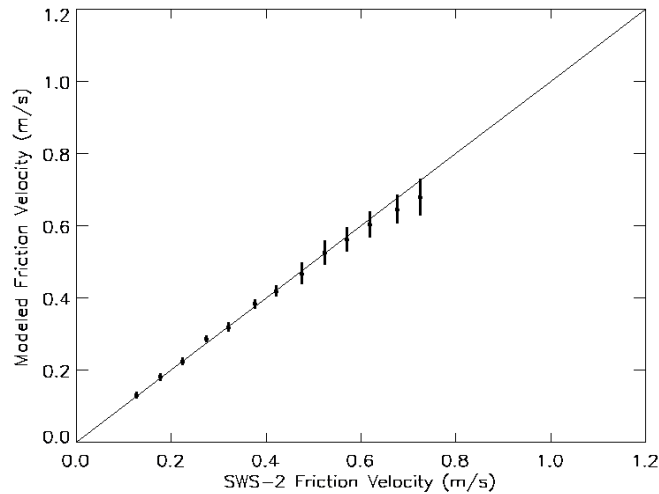


Figure 2: Comparison of modeled and observed SWS-2 friction velocity magnitudes, shown as means and uncertainty in those means. The error bars indicate ± 3 standard deviations in the mean. There are only 10 points in each of the two bins for the extreme means, whereas there are 22 to 104 points in the other bins. The bin-width for SWS-2 u_* values is 0.05 ms^{-1} , and means are calculated only when there are at least 8 values in a bin.

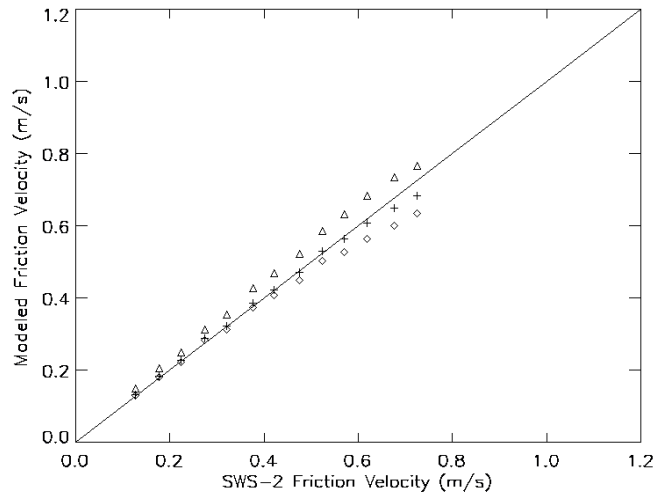


Figure 3: Comparison of modeled influences of orbital velocity and displacement height on friction velocity in the SWS-2 data. The modeled friction velocity considering both influences (denoted +) is approximately 10 to 12% less than when orbital velocity is not considered (denoted Δ); and is slightly larger than when displacement height is ignored (denoted \diamond).

6 Applications to scatterometry

One of the early goals of scatterometry was to remotely sense ocean vector surface stress. The above results indicate that this goal might be close to being realized. The calibration of radar backscatter to equivalent neutral winds deals with the dependence of stress on atmospheric stability. However, wave characteristics also influence surface turbulent stress. The dependence of the calibration on the horizontal vector of the dominant waves' orbital velocity accounts for much of the dependency on wave characteristics. Scatterometers clearly respond to wind speed minus a fraction of the orbital velocity; however, it is not certain that this fraction is equal to f (from Eqn 10), which describes the influence of waves on the relation between earth-relative winds and stress. If the influence of orbital velocity on scatterometer wind speeds is similar in magnitude to f , then scatterometers can easily be used to estimate surface stress,

as well as the surface stress derivatives that are of great importance to ocean forcing. If the above case occurs, then this estimate of stress will be accurate so long as the influence of displacement height can be ignored. The overestimation that occurs due to ignoring the displacement height is less than 10% for SWS-2 wind speeds less than approximately 20ms^{-1} . This range of wind speeds accounts for the vast majority of ocean winds, including most winds associated with storms.

It seems likely that the mean influence of displacement height could be considered to further reduce bias in satellite-based estimates of surface stress for extreme conditions. Ideally, surface stress and wave observations could be obtained for such conditions, so that the above model could be either validated or improved for extreme conditions. It is interesting to note that the orbital velocity modification could account for several seemingly conflicting observations in hurricanes: surface winds that are extrapolated downward are found to have greater values than are consistent with a log-wind profile with zero surface wind and the associated estimated surface stress. The orbital velocity could account for a much larger than expected near-surface wind speed, for such extreme conditions.

7 Conclusions

The influence of wave characteristics on surface stress has been examined. Previous approaches have modified the momentum roughness length; however, the approach described here allows for a simple Charnock parameterization of momentum roughness length. The influences of waves are considered in the lower boundary condition in the modified log-wind profile. The horizontal component of the dominant waves' orbital velocity modifies the near surface boundary condition for wind velocity. Eighty percent of this horizontal component is vector-subtracted from the near surface wind speed. Typically this modification decreases the vertical wind shear and thereby also decreases the wind stress. However, if the waves are propagating against the wind direction there will be an increase in the wind shear and an increase in the surface turbulent stress. This boundary condition on velocity is matched with a boundary condition related to the vertical coordinate system, implying a non-zero displacement height. This knowledge provides the information for a first estimate of the displacement height, representing a vertical offset of the log-wind profile. The displacement height for wind waves is found to be 80% of the significant wave height. Some caution must be taken in applying these results to conditions where the waves are dominated by swell. The influence of the orbital velocity on stress has been verified with observations; however, the value of the displacement height has not been adequately studied for these conditions.

Nevertheless, for very high wind speeds, the consideration of displacement height helps to reduce a systematic underestimate of the surface turbulent stress.

Acknowledgments. I thank Peter Taylor for providing the SWS-2 data and advice on quality assurance. COAPS receives its base funding from ONR's Secretary of Navy Grant to James J. O'Brien. Current support is from NASA's Ocean Vector Winds Science Team, OSU's SeaWinds project, Florida State University's First Year Investigator Program, NOPP, and the NSF.

References

- [1] Schlax, M.G., Chelton, D.B. & Freilich, M.H. Sampling errors in wind fields constructed from single and tandem scatterometer datasets, *J. Atmos. Oceanic Technol.*, **18**, pp. 1014-1036, 2001.
- [2] O'Brien, J. J., and others, Scientific opportunities using satellite wind stress measurements over the ocean. Report of S3 Working Group, *Nova University Press*, 153 pp, 1982.
- [3] Powell, M.D., Vickery, P.J., & Reinhold, T.A., Reduced drag coefficient for high wind speeds in tropical cyclones. *Nature*, **422**, 279-283, 2003.
- [4] Shuyi Chen, personal communication, 2003)
- [5] Kusaba, T., & Masuda, A. The roughness height and drag law over the water surface based on the hypothesis of local equilibrium. *J. Phys. Ocean. Soc. Japan*, **44**, 200–214, 1988.
- [6] Geernaert, G.L. Measurements of the angle between the wind stress vector in the surface layer over the North Sea. *J. Geophys. Res.*, **91**, pp. 7667–7679, 1990.
- [7] Toba, Y., Ida, N., Kawamura, H., Ebuchi, N., & Jones, I.S.F. Wave dependence of sea-surface wind stress. *J. Phys. Oceanogr.*, **20**, pp. 705–721, 1990.
- [8] Perrie W., & Toulany, B. Fetch relations for wind-generated waves as a function of wind-stress scaling. *J. Phys. Oceanogr.*, **20**, pp. 1666–1681, 1990.
- [9] Maat, M., Kraan, C. & Oost, W.A. The roughness of wind waves. *Bound.-Layer Meteorol.*, **54**, pp. 89–103, 1991.
- [10] Smith, S.D., Anderson, R.J. Oost, W.A. Kraan, C. Maat, N. DeCosmo, J. Katsaros, K.B. Davidson, K.L. Bumke, K. Hasse, L. & Cadwick, H.M. Sea surface wind stress and drag coefficients: the HEXOS results. *Bound.-Layer Meteorol.*, **60**, pp. 109–142, 1992.

- [11] Yelland, M. J., Moat, B.I., Taylor, P.K., Pascal, R. W. Hutchings, J. & Cornell, V. C. Wind stress measurements from the open ocean corrected for airflow distortion by the ship. *J. Phys. Oceanogr.*, **28**, pp. 1511–1526, 1998.
- [12] Bourassa, M. A., Vincent, D.G., & Wood, W.L. A flux parameterization including the effects of capillary waves and sea state. *J. Atmos. Sci.*, **56**, pp. 1123-1139, 1999.
- [13] Bourassa, M.A. An Improved Seastate Dependency For Surface Stress Derived from *In Situ* and Remotely Sensed Winds. *Advances in Space Res.*, **33**(7), pp. 1136-1142, 2004.
- [14] Taylor, P.K., & Yelland, M. J. The dependence of sea surface roughness on the height and steepness of the waves, *J. Phys. Oceanogr.*, **18**, pp. 572–590, 2001.
- [15] Quilfen Y., Chapron, B. & Vandemark, D. The ERS scatterometers wind measurement accuracy: evidence of seasonal and regional biases. *J. Atmos. Oceanic Technol.*, **18**, pp. 1684–1697, 2001.
- [16] Katsaros, K.B., & Brown, R.A. Legacy of SeaSat mission for studies of the atmosphere and air-sea-ice interactions. *Bull. Amer. Meteor. Soc.*, **72**, pp. 967-981, 1991.
- [17] Naderi, F.M., Freilich, M.H. and Long, D.G. Spaceborne radar measurements of wind velocity over the ocean- an overview of the NSCAT scatterometer system. *Proceedings of the IEEE*, **79**, pp. 850-866, 1991.
- [18] M. H. Freilich and D. G. Long, personal communication, 1998.
- [19] Zecchetto, S, Tando, I. & Quilfen, Y. The CERSAT dealiasing of ERS-2 scatterometer winds in the Mediterranean Sea. *CERSAT News*, Scientific topic number 2, pp. 1-4, 1999.
- [20] Weissman, D.E., Bourassa, M.A., & Tongue, J. Effects of rain-rate and wind magnitude on SeaWinds scatterometer wind speed errors. *J. Atmos. Oceanic Technol.*, **19**, pp. 738–746, 2002.
- [21] Bliven, L.F., Branger, H., Sobieski, P.C. & Giovanangeli, J-P. An analysis of scatterometer returns from a water surface agitated by artificial rain. *International Journal of Remote Sensing*, **14**, pp. 2315-2329, 1993.
- [22] Sobieski, P., & Bliven, L.F. Analysis of high speed images of raindrop splash products and ku-band scatterometer returns. *International Journal of Remote Sensing*, **16**, pp. 2721-2726, 1995.
- [23] Sobieski, P.W., Craeye, C., & Bliven, L.F. Scatterometric signatures of multivariate drop impacts on fresh and salt water surfaces. *International Journal of Remote Sensing*, **20**, pp. 2149-2166, 1999.
- [24] Weissman, D.E., Bourassa, M.A., Tongue, J., & O'Brien, J.J. Calibrating the QuikSCAT/SeaWinds Radar for Measuring Rain Over Water. *IEEE Trans. Geosci. Remote Sens.*, **41**, pp. 2814-2820, 2003.

- [25] Yueh, S.H., Styles, B., & Liu, W.T. QuikSCAT Wind Retrievals for Tropical Cyclones, *IEEE Trans. Geosci. Remote Sens.*, **41** 2616- 2628, 2003.
- [26] Draper, D.W., & Long, D.G. Evaluating the Effect of Rain on SeaWinds Scatterometer Measurements, *J. Geophys. Res.*, **109**(C02005), doi:10.1029/2002JC001741, 2004.
- [27] Freilich, M.H., & Dunbar, R.S. The accuracy of the NSCAT 1 vector winds: Comparison with National Data Buoy Center buoys. *J. Geophys. Res.* **104**, pp. 11231-11246, 1999.
- [28] Wentz, F.J., & Smith, D.K. A model function for the ocean-normalized radar cross section at 14 GHz derived from NSCAT observations. *J. Geophys. Res.*, **104**, pp. 11499-11514, 1999.
- [29] Stoffelen A., Toward the true near-surface wind speed: Error modeling and calibration using triple collocation. *J. Geophys. Res.*, **103**, pp. 7755 – 7766, 1998.
- [30] Bourassa, M.A., Legler, D.M. O'Brien, J.J. & Smith, S.R. SeaWinds Validation with Research Vessels, *J. Geophys. Res.*, **108**, 3019, DOI 10.1029/2001JC001081, 2003.
- [31] Cardone, V.J. Specification of the wind distribution in the marine boundary layer for wave forecasting. *Geophys. Sci. Lab. N.Y. Univ. Report TR-69-1* (NTIS AD 702-490), 1969.
- [32] Ross, D. B., Cardone, V.J., Overland, J., McPherson, R.D. Pierson, W.J. Jr., & Yu, T., Oceanic surface winds. *Adv. Geophys.*, **27**, pp. 101-138, 1985.
- [33] Cardone, V.J., Jensen, R.E., Resio, D.T., Swail V.R. & Cox, A.T. Evaluation of contemporary ocean wave models in rare extreme events: the "Halloween Storm" of October, 1991 and the "Storm of the Century" of March 1993. *J. Atmos. Oceanic Technol.*, **13**, pp. 198-230, 1996.
- [34] Verschell, M.A., Bourassa, M.A. Weissman, D.E. & O'Brien, J.J. Model validation of the NASA scatterometer winds, *J. Geophys. Res.*, **104**, pp. 11,359–11,374, 1999.
- [35] Dobson, F.W., Anderson, R.J. Taylor, P.K. & Yelland, M.J. Storm Wind Study II: Open ocean wind and sea state measurements. *Proc. Symp. on the Wind-Driven Air-Sea Interface: Electromagnetic and Acoustic Sensing, Wave Dynamics and Turbulent Fluxes*, M. L. Banner, Ed., University of New South Wales, pp. 295-296, 1999.
- [36] Taylor, P.K., Yelland, M.J., Dobson, F.W., & Anderson, R.J. Storm Wind Study II: Wind stress estimates from buoy and ship. *Proc. Symp. on the Wind-Driven Air-Sea Interface: Electromagnetic and Acoustic Sensing, Wave Dynamics and Turbulent Fluxes*, M. L. Banner, Ed., University of New South Wales, pp. 353-354, 1999.
- [37] P. K. Taylor, personal communication, 2003.

- [38] Liu, W.T., Katsaros, K.B., Businger, J.A. Bulk parameterization of air-sea exchanges of heat and water vapor including the molecular constraints at the interface. *J. Atmos. Sci.*, **36**, pp. 1722–1735, 1979.
- [39] Clayson, C.A., Fairall, C.W. & Curry, J.A. Evaluation of turbulent fluxes at the ocean surface using surface renewal theory, *J. Geophys. Res.*, **101**, pp. 28,503–28,513, 1996.
- [40] Charnock, H., Wind stress on a water surface. *Quart. J. Roy. Meteor. Soc.*, **81**, pp. 639–640, 1955.
- [41] Taylor, P. K., personal communication, 1999.
- [42] Nikuradse, J., *Stromungsgesetze in rauhen Rohren*. V. D. I. Forschungsheft 361, 22 pp., 1933.
- [43] Kondo, J., Air–sea bulk transfer coefficients in diabatic conditions. *Bound.–Layer Meteorol.*, **9**, pp. 91–112, 1975.
- [44] Okuda, K., Kawai, S. & Toba, Y. Measurements of skin friction distribution along the surface of wind waves. *J. Oceanog. Soc. Japan*, **33**, pp. 190–198, 1997.
- [45] Günther, H., and others Technical Report No. 68: Implementation of a third generation ocean wave model at the European Centre for Medium–Range Weather Forecasts, European Centre for Medium–Range Weather Forecasts, pp. 34, 1992.
- [46] Janssen, P.A.E.M. Wave-induced stress and the drag of airflow over sea waves. *J. Phys. Oceanogr.*, **19**, pp. 745–754, 1989.
- [47] Janssen, P.A.E.M. Quasi–linear theory of wind–wave generation applied to wave forecasting. *J. Phys. Oceanogr.*, **21**, pp. 1631–1642, 1991.
- [48] Donelan, M.A., Drennan, W.M. & Katsaros, K.B., The air-sea momentum flux in conditions of wind sea and swell. *J. Phys. Oceanogr.*, **27**, pp. 2087–2099, 1997.